International Journal of Advance Research in Science and Engineering
Volume No. 15, Issue No. 01, January 2026
www.ijarse.com
IJARSE
ISSN 2319 - 8354

ELECTRONIC STRUCTURE OF LAYERED HfS_2 INVESTIGATED THROUGH ARPES AND POTASSIUM DOPING

Kousik Pramanik[1], Dr. Aloke Verma[2]

[1,2] Department of Physics, Kalinga University, Raipur (CG), India

ABSTRACT

The distinctive structural and electrical characteristics of layered transition metal dichalcogenides, such as HfS_2, have garnered considerable interest. In this research, the electronic structure of layered 1T-HfS_k is investigated by means of theoretical calculations and angle-resolved photoemission spectroscopy. The surface-level potassium doping of HfS_2 allowed for a fine-tuning of its band structure, revealing the valence and conduction bands with remarkable clarity. The results demonstrate that the energy bands are progressively shifted and the conduction band is made more apparent by electron doping. Furthermore, in order to comprehend their impact on electrical behavior, sulfur vacancy defects were engineered using controlled post-annealing. These flaws were found to cause a considerable distortion and other alterations in the conduction band close to the M point. The indirect band gap character of HfS_2 is confirmed by experimental results, which are in close accord with theoretical expectations. For the purpose of developing more sophisticated devices, this study sheds light on the ways in which doping and flaws can alter the electrical characteristics of layered materials.

Keywords: Electronic band, Potassium, Sulfur, Energy, Layered

I.INTRODUCTION

The study of two-dimensional (2D) materials is now among the most fascinating and dynamic subfields of nanotechnology and materials science. These materials' electrical, physical, and chemical characteristics are radically different from those of their bulk equivalents due to the atomically thin layers that make them up. Because of its unique properties—such as its high electrical conductivity, mechanical strength, carrier mobility, and thermal stability—graphene has attracted the greatest interest among the 2D materials found thus far. Because of these characteristics, graphene has emerged as a game-changing material that might revolutionize several industries, including electronics, energy storage, sensors, and flexible gadgets. Graphene has many great qualities, but it has one big drawback—it has zero bandgap. To accomplish effective switching between the ON and OFF states in electrical devices like field-effect transistors (FETs), a limited bandgap is necessary. Digital electronics and optoelectronic systems find graphene's limited use because to its difficulty in controlling current flow

caused by the absence of this bandgap. Consequently, scientists are now looking at other two-dimensional materials with an inherent bandgap, which would make them better for device construction.

Because of this, materials like black phosphorus, hexagonal boron nitride (h-BN), and transition metal dichalcogenides (TMDs) have become more popular. Depending on their thickness and composition, these materials can display adjustable optical and electrical characteristics, in addition to offering a natural bandgap. Of them, TMDs have risen to prominence owing to their adaptability and breadth of use. A common chemical formula for transition metal dichalcogenides (TMDs) is MX_2, where M is a transition metal (e.g., zirconium, hafnium, or molybdenum) and X is a chalcogen element (e.g., sulfur, selenium, or tellurium). These materials are ideal for nanoscale device engineering because they may be found in either monolayer or few-layer forms, and their characteristics can change dramatically with thickness.

Group VIB materials of the TMD family, including MoS_k and WS_k, have been the subject of a great deal of research during the last 10 years. Transistors, photodetectors, solar cells, and flexible electronics are just a few of the many areas where these materials have shown great promise. As an example, the optical characteristics of MoS_2 are much improved when it is grown into a monolayer because its bandgap changes from an indirect one in bulk to a direct one. Group VIB TMDs have emerged as the go-to materials for research into 2D semiconductors because of these benefits.

Mechanical exfoliation methods were initially used by researchers to generate thin layers of HfS_2. To get flawless flakes, this method entails utilizing sticky tapes to peel layers off of bulk crystals. Based on few-layer HfS_2, this approach has been used in several research to fabricate efficient field-effect transistors and ultrasensitive phototransistors. Nevertheless, there are a number of limits to mechanical exfoliation. The resultant flakes are frequently uneven in thickness and do not permit accurate control over the layer count. Systematic research are made more difficult and large-scale device production is hindered by this lack of homogeneity.

In response to these difficulties, chemical vapor deposition (CVD) has been proposed as a viable method for producing 2D materials across wide areas with precisely regulated thickness and excellent crystallinity. Monolayers of materials including MoS_k, WS_k, and ZrS_k have been grown on different substrates using CVD. This method allows for more precise regulation of growth conditions, which in turn facilitates the manufacture of consistent, scalable films well-suited for use in industrial settings.

There have been recent endeavors to cultivate HfS_2 using CVD methods. Particularly noteworthy is the demonstration of epitaxial development of high-quality HfS_2 films on c-plane sapphire substrates. Although this is a big step forward, it is still not easy to get the best performance out of these films for

devices. The inherent material characteristics of HfS_2 are one of the primary concerns. The interaction energy of HfS_2 is around 1.33 eV per primitive cell, which is greater than that of other TMDs like MoS_2, which has an interaction energy of about 0.46 eV. The growth dynamics during CVD are impacted by this increased contact, which in turn changes the substrate's surface energy.

This prevents the adatoms from moving freely across the substrate and forming the intended horizontal layers, but instead causes them to arrange themselves vertically. When it comes to electrical and optoelectronic applications, where a seamless planar structure is key for effective charge transfer and device integration, films with a vertical alignment just don't cut it.

The inability to directly develop HfS_2 on technologically significant substrates like SiO_2/Si is another significant obstacle. Integrating 2D materials into current electrical device topologies requires this sort of substrate, which is utilized extensively in the semiconductor industry. Nucleation, surface energy mismatch, and growth kinetics are some of the challenges that have made direct growth of HfS_k on SiO_2/Si employing CVD a challenging task.

One prevalent method now is to produce HfS_k on sapphire surfaces, and then to use dry or wet transfer procedures to transfer the films onto SiO_2/Si substrates. There are a number of undesirable side effects that come with this approach, even if it does enable device creation to some extent. Material contamination, structural damage, strain, and accidental doping are all possible outcomes of the transfer procedure. These variables have the potential to greatly change the intrinsic electrical characteristics of HfS_k, which in turn makes it hard to research its behavior precisely and limits its use in real-world applications.

The band structure, carrier mobility, and overall stability of the material can be altered by the introduction of strain and contaminants during transfer. This is a significant obstacle for scientists working on HfS_2-based systems that aspire to be dependable and perform well. Consequently, better synthesis methods are urgently required to allow the direct development of high-quality HfS_2 films on appropriate substrates, bypassing the necessity for transfer steps.

Along with development problems, another crucial factor that demands careful attention is limiting flaws in HfS_2. The optical and electrical characteristics of a material can be drastically altered by defects like sulfur vacancies. While it's true that some flaws can actually improve performance in particular contexts, having too many or not controlling them might lead to devices underperforming. Thus, in order to maximize the HfS_k characteristics, it is crucial to comprehend and manage the production of defects.

II.REVIEW OF LITERATURE

Cao, Yong et al., (2022) By employing first-principles computations, we probe the electrical structure of the HfS2/PtSSe heterojunction in great detail. By positioning holes at HfS2 and electrons at PtSSe, the HfS2/PtSSe heterostructure exhibits an intrinsic type-II band alignment. The segregated charge distribution effectively prevents carrier recombination. The HfS2/PtSSe heterojunction has a substantially greater absorption of visible and ultraviolet light compared to the individual PtSSe and HfS2 monolayers. It is also possible to linearly alter the bandgap of the heterojunction using the bi-axial strain. The heterojunction can change from a type-II to a type-III band alignment, specifically when the compress strain strength is 9%. It is the increased hybridization of the Hf-5d and Se-4p states that causes the heterojunction bandgap to change under compressed pressure. Thanks to its adjustable bandgap, the HfS2/PtSSe heterojunction shows potential as a high-performance tunable optoelectronic nanodevice competitor..

Neal, S et al., (2021) Using infrared absorption and Raman scattering spectroscopies, we study the properties of the heavy transition metal dichalcogenide 1T-HfS2. Utilizing the LO-TO splitting of the Eu vibrational mode in combination with a reassessment of mode mass, unit cell volume, and dielectric constant, we determine the Born effective charge. Our results show that ZB* = 5.3e agrees with the additional first-principles computations. Separating Born charge into polarizability and local charge, we also resolve the controversy about the chemical bonding character of this system. We find that Z* is equal to 5.2e and α equals 5.07 Å3. Sulfur p to hafnium d charge transfer, produced by polar displacement, causes the Born charge to be higher than hafnium's typical 4+. This means that 1T-HfS2 is a strong covalent effect ionic crystal. Our results, taken as a whole, lay the framework for understanding the vibrational properties of 1T-HfS2 and open the door to learning about its tubes and sheets.

Najmaei, Sina et al., (2020) The ability to alter material properties on the fly is crucial for the realization of new paradigms in neuromorphic and quantum computing. The unique structure of van der Waals layers allows for this targeted reconfigurability to be achieved through a long-term process. Our electrochemical intercalation of organometallics-based approach to controlling the electron and phonon behavior in hafnium disulfide is both efficient and adaptable. Both theoretical and practical analyses of the intercalated material's physical properties have revealed a discernible and substantial change. Furthermore, the slight chemical interactions between the organometallics and hafnium disulfide enable an electric-field driven intercalant drift and charge-discharge mechanism. By manipulating the organometallic composition in this way, hafnium disulfide can have a cross-plane electrical conductivity that is 400 times adjustable (1.8 μS/cm-741 μS/cm) and a cross-plane thermal conductivity

that is 4 times adjustable (0.35 $Wm^{-1} K^{-1}$-1.45 $Wm^{-1} K^{-1}$). Our study uncovered a complete strategy for dynamically designing layered-material features for high-performance electrical and phononic applications.

Singh, Deobrat, et al., (2018) investigated the optical, electrical, and structural properties of Frenkel and Schottky defects in monolayer HfS2 using first-principles models. Our observations point to the possibility of modulating the electronic band gap, which in turn can alter electrical and optical properties including the dielectric function and optical absorption spectra. The electronic band gaps in pure monolayer HfS2 are 1.26 eV, those in monolayers with Frenkel defects are 0.28 eV, and those in monolayers with Schottky defects are 1.49 eV. Our findings suggest that a structural defect in the production of ultra-high-quality monolayer hafnium disulphide can be used to modify its optical and electrical properties, opening up new avenues for future applications in optoelectronics, spintronics, and high-performance electronic devices.

Lu, Haichang et al., (2018) The carrier mobilities of monolayer HfS2 and SnS2 are significantly higher than those of MoS2, which has a straight bandgap. Their band offsets render them perfect for use in field-effect transistors (FETs) when coupled with WSe2. We study the effective masses, defects, and substitutional dopants of these dichalcogenides in this paper. Even though HfS2 has an ionic appearance, its effective masses are quite small. The S vacancy in SnS2 is deeply embedded, whereas in HfS2 it is only partially filled. The results reveal a very minor presence of substitutional dopants at the S location. With MoS2 and black phosphorus, things are different since the donors and acceptors aren't always shallow and dopants can rearrange themselves into deep non-doping topologies. When compared to MoS2, HfS2 is preferable for semiconductor processing due to its easier CVD precursors for making HfO2.

Iordanidou, Konstantina et al., (2016) Several point defects in single-layer HfS2 are studied in this study for their electrical, structural, and energetic properties using first-principles calculations. Our results show that lattice defects may significantly change the electrical structure of HfS2 by introducing defect states into the gap and pinning the Fermi level. We also analyze the oxidation of pristine and S deficient monolayers using first-principles molecular dynamics calculations. The material's electron effective mass and energy bandgap are increased when O atoms are substituted for S atoms in the lattice, forming strong Hf-O bonds. In conclusion, our results provide new insight on HfS2-based field effect transistor oxidation and highlight the need of defect control for future high-performance device fabrication.

III.EXPERIMENTAL SETUP

Iodine was used as a transfer agent in the chemical vapor transport technique to generate the 1T-HfS2 crystals. Mixed with iodine and sealed in a quartz tube under a vacuum of approximately 10−4 Pa were stoichiometric Hf (99.9%) and S powder (99.9%). A dual-temperature zone tube furnace was used to install the assembly. Ten50 ◦C was maintained at one end of the quartz tube containing the initial ingredients, while 970 ◦C was maintained at the other end for crystal formation. The cold end of the quartz tube yielded big HfS2 crystals after two weeks. After growing the HfS2 in vacuum, it was post-annealed at 500 °C for varying durations to produce defective samples with S vacancies.

An ARPES that was constructed at home was used to study the electronic structures of HfS2. The photoelectron excitation source was a helium discharge lamp, and the photon energy was 21.2 eV. To prevent the HfS2 samples from being degraded while the H20E silver-filled epoxy cured, they were produced in a glove box with an argon atomosphere that is highly purified. This was done in order to conduct ARPES measurements. To get new HfS2 surfaces for ARPES measurements, the samples were cut on the spot along the (001) plane in a vacuum with a pressure greater than 10−8 Pa while the material was still at room temperature. Additionally, the ARPES measurements were conducted at ambient temperature. A common commercial alkali-metal dispenser was used to deposit potassium (K) alkali metal on-site.

Using the density-functional theory (DFT) implemented in the QUANTUM ESPRESSO code, relativistic first-principles calculations were performed to derive the theoretical electronic structures of HfS2. In order to get a dependable gap that is in agreement with the experimental results, the calculations utilized a hybrid functional approximation for the exchange-correlation term, Heyd-Scuseria-Ernzerhof (HSE06). Layered materials often exhibit weak van der Waals forces, which may be described using the dispersion corrected DFT-D3.

We settled on 50 Ry as the cutoff energy for the wave function and 400 Ry as the cutoff energy for the charge density. A grid measuring 8 × 8 × 4 was used to sample the Brillouin zone. A first-principles tight-binding model Hamilton based on maximally localized Wannier functions was built by fitting the DFT band structures with the WANNIER90 algorithm; this allowed us to acquire the band structure and surface spectra. For the first projection, the Hf-d and S-p orbitals were utilized. The WANNIERTOOLS package's Greens function approach was used to compute the surface spectra of HfS2.

IV.RESULTS AND DISCUSSION

As shown in figure 1(a), the lattice parameters for HfS2 are a = b = 3.64 Å, c = 5.86 Å, α = 90°, and β

= 120°, and the crystallization form is a CdI2-PbI polytype structure (space group P3¯ m1). The structure is made up of atomic layers that are sandwiched between sulfur and hafnium, with the hafnium atoms located in the middle. Using a 532 nm laser excitation, Figure 1(b) displays the Raman spectra of the as-grown and faulty post-annealed HfS2. The Eg mode, which appears at 256 cm−1, is caused by the in-plane vibration of S atoms, while the A1g mode, which appears at 336 cm−1, is caused by the out-plane vibration of S atoms. Hence, the Raman spectra of perfect and imperfect HfS2 containing S vacancies are indistinguishable.

No noticeable alterations in the crystal structure of HfS2 are shown by the XRD θ-2θ scan patterns on the easy-cleaved (001) surface of both the as-grown and faulty post-annealed samples, as shown in Figure 1(c). In contrast, x-ray photoelectron spectroscopy (XPS) may be employed to identify and differentiate between perfect and imperfect HfS2, as seen in figures 1(d-e). The as-grown HfS2 can be considered pure S2 because its XPS spectrum [figure 1(d)] only shows two peaks of Hf 4f, with peaks at 17.18 eV for the Hf 4f7/2 state and 18.84 eV for the Hf 4f5/2 state.

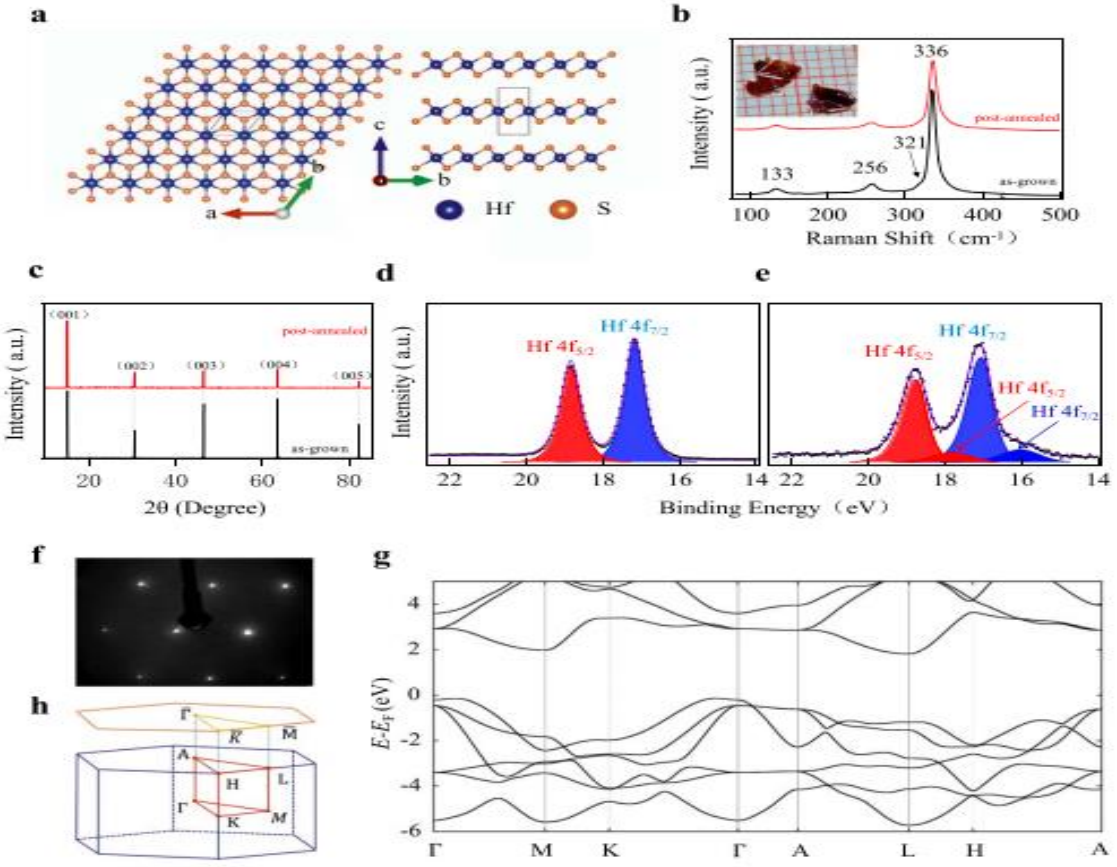

Figure 1: Comprehensive Structural, Spectroscopic, and Electronic Characterization of Layered HfS_2 Crystals

These spectra match the standard spectra for HfS2 crystal. On the other hand, Figure 1(e) shows the XPS spectrum of defective HfS2. In addition to the two primary peaks observed in a pure HfS2 environment, two additional minor peaks at 16.05 eV and 17.79 eV are observed in an environment with S vacancy defects; these may be identified as 4f7/2 and 4f5/2 of Hf, respectively. The reduction in binding energies for Hf 4f7/2 and Hf 4f5/2 is due to the fact that the chemical environment of some Hf atoms will change as a result of the S vacancies in HfS2. The conductivity of MoS2 and HfO2 is comparable. Displayed in Figure 1(f) is the LEED pattern of the cleaved surface of HfS2. A flat, well-ordered surface is shown by the crisp and distinct diffraction spots, which confirms that the as-grown HfS2 is of good quality. The computed bulk bands of HfS2 along several high-symmetry pathways are shown in Figure 1(g). The valence band maximum (VBM) is located at the Γ point while the conduction band minimum (CBM) is located around the L point, creating an indirect gap in HfS2.

To begin, as shown in figure 2, the electronic structures of the as-grown HfS2 were measured using ARPES. The constant energy mapping of HfS2 is displayed in Figures 2(a)-(c) for three chosen binding energies, namely −1.6 (about VBM), −2.7, and −3.0 eV. The band dispersions of HfS2 measured in the K -G and M -G directions are shown in Figures 2(e)-(f), respectively. Based on the ARPES data, we can observe that the Fermi level is located in the indirect gap and the VBM is approximately at the binding energy of −1.5 eV. It should be noted that the VBM values observed by ARPES are consistently lower than the one obtained theoretically. There might be a pair of explanations for this. To start with, the theoretical computation gives an inflated value for the VBM and a low value for the Fermi level. Secondly, as can be seen in figure 1(d), even if the S vacancy defects do not show up in the XPS spectrum, there are still some in the perfect samples. Due to electron doping caused by S vacancy defects, the Fermi level is raised and the VBM is lowered. Band structures of HfS2 derived from ARPES measurements and theoretical simulations agree well with respect to all parameters except relative energy. This was demonstrated by a 1.05 eV reduction in the binding energy of the computed findings. The computed constant energy mapping in figure 2(d) faithfully replicates the matching ARPES result in figure 2(c), as is evident. The computed bands from the ΓKM plane ($k_z = 0$, red dashed curves) and the AHL plane ($k_z = \pi$, white dashed curves) clearly illustrate the primary characteristics of the ARPES observed band dispersions, as seen in figures 2(g) and 2(h). It is usual in ARPES studies with low excitation photon energy for the kz broadening effect to coexist in one ARPES-measured picture, which is why the bands from the $k_z = 0$ plane and the $k_z = \pi$ plane coexist. For photon energy hv = 21.2 eV, our work indicates that the probing depth λ is around 5 Å. The length of kz in the first Brillouin zone of HfS2, which is about $2\pi/\lambda \sim 1$ Å^{-1}, may be approximated by the Heisenberg uncertainty principle as $\Delta k_z = 2\pi/\Lambda$. Since ARPES measurements incorporate the bands over the whole kz window, the kz broadening effect encompasses the entire Brillouin zone. Additional details may be seen in figures 2(i)

and 2(j), which compare the band dispersions observed by ARPES with the surface spectra computed using kz-integrated bulk bands. This shows that the theoretical calculations and the ARPES observations are in good agreement.

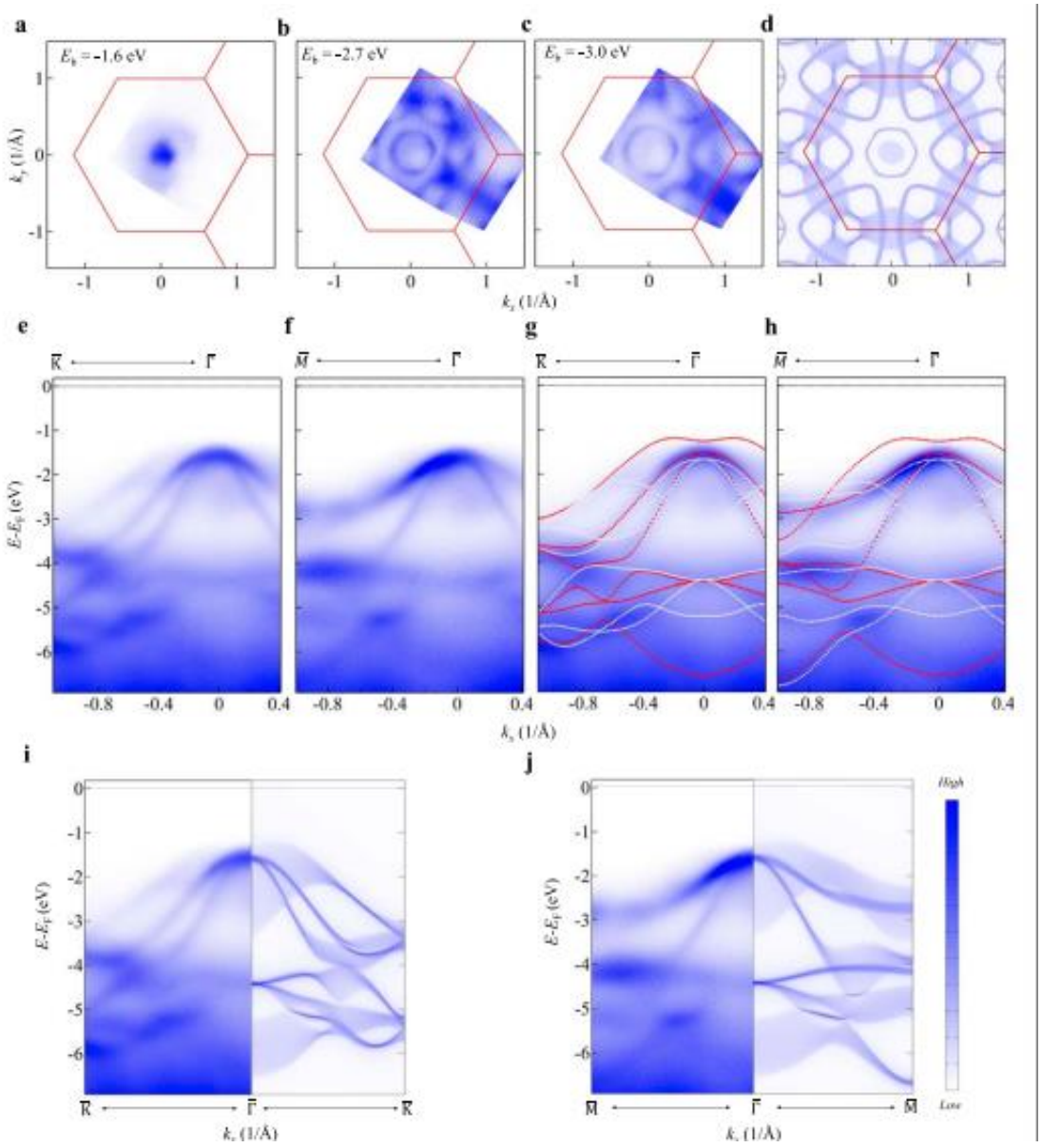

Figure 2: ARPES and Theoretical Electronic Band Structure Mapping of HfS_2

By tuning the band structures of HfS2, researchers were able to get insight into its indirect band gap and conduction bands. This was achieved by the in-situ deposition of the alkali metal potassium (K) on cleaved HfS2 surfaces. The changes in the band structures of HfS2 as a function of time exposed to potassium deposition are illustrated in figure 3(a). After electron doping, the bands as a whole gradually decrease until saturation is achieved, at which point the VBM drops to around -2.23 eV. When electrons

are introduced into a material, they occupy conduction bands that were previously vacant, allowing ARPES to detect them. After surface potassium doping saturation, the band dispersions of HfS2 along G-M are shown in Figure 3(b), with the gray box indicating the location of the CBM. Figure 3(b) shows that compared to the valence bands, the conduction bands have a substantially lower spectrum weight. Clearly visible in figure 3(c), an expanded and contrast-enhanced picture of the CBM's surroundings crosses the Fermi level with a parabolic-like band. The calculated values for the CBM in figure 3(c) and the VBM in figure 3(b) are about −0.12 eV and ~−2.23 eV, respectively. So, according to the results from ARPES, the indirect gap of HfS2 is around 2.11 eV. After the surface potassium doping saturation, figure 3(d) shows the Fermi surface mapping of HfS2. Figure 3(e) shows that theoretical calculations faithfully recreate the ellipsoidal electron pockets centered at M points, which are generated by the conduction bands around M points.

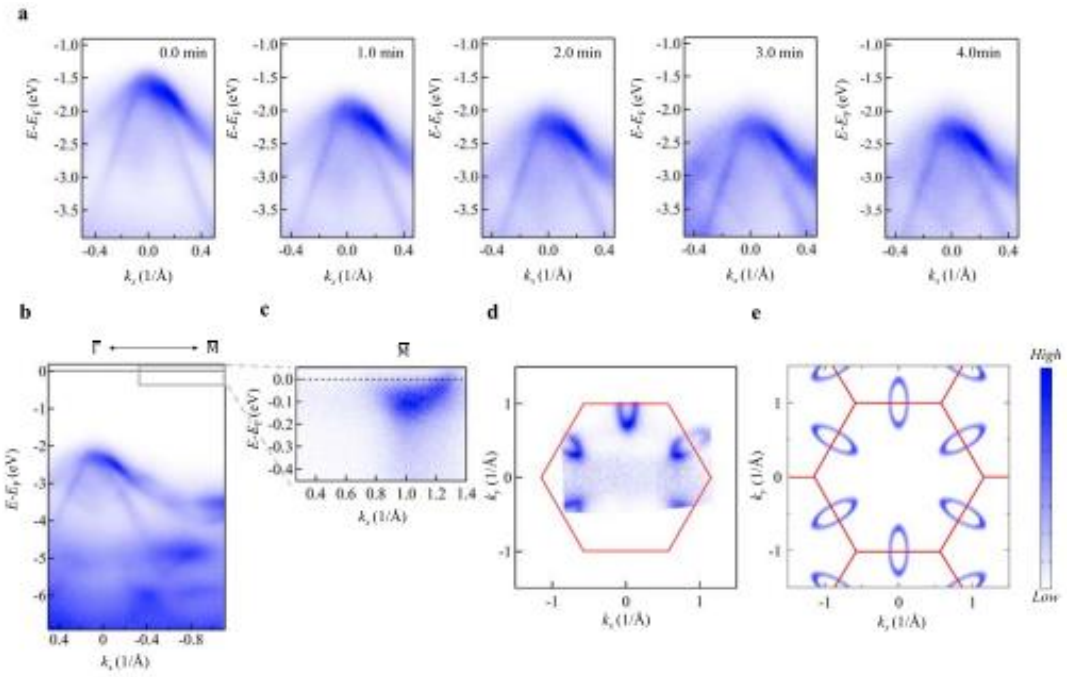

Figure 3: Effect of Surface Potassium Doping on the Electronic Structure of HfS_2

V.CONCLUSION

This work elucidates the electrical structure of HfS_2 and demonstrates how doping and defect engineering may affect it. While annealing generated sulfur vacancies, which caused obvious alterations, especially around the conduction band minimum, potassium doping successfully shifted the energy bands and revealed the conduction band. The results are more credible since they are in line with theoretical calculations and experimental data. In conclusion, the study shows that flaws and external tuning techniques are key to customizing layered materials' characteristics, which makes HfS_2 an

attractive material for future electrical and optoelectronic devices.

REFERENCES: -

[1] Foucher, W. Mortelmans, R. Dana, K. Reidy, B. Wu, Z. Sofer, R. Jaramillo, and F. Ross, "Investigation of oxidation mechanisms in HfS_2 and ZrS_2 via in situ electron microscopy," *The Journal of Physical Chemistry C*, vol. 129, no. 51, pp. 1-15. 2025.

[2] Y. Lin, S. Xiao, X. Zhang, W. Liu, Y. He, Z. Zhou, X. Yang, S. Zhang, S. He, Y. Guo, and Y. Zhao, "Defects induced changes in conduction bands of HfS_2," *Physica Scripta*, vol. 99, no. 3, pp. 1–8, 2024.

[3] Inamdar, N. Som, S. Dabhi, A. Pratap, P. Spiewak, K. J. Kurzydłowski, and P. Jha, "A striking exploration of defect engineering in HfS_2, $HfSe_2$, and Janus HfSSe through ab initio analysis for HER catalysis application," *International Journal of Hydrogen Energy*, vol. 68, no. 1, pp. 268–276, 2024.

[4] T. Sheikh, "Defect engineered magnetism induction and electronic structure modulation in monolayer MoS_2," *Heliyon*, vol. 10, no. 1, pp. e23384, 2023.

[5] Y. Cao, X. Zhu, D. Zou, W. Sheng, and Y. Xu, "Investigation of two-dimensional HfS_2/PtSSe heterostructure with strong visible light adsorption and strain tunable bandgap," *Journal of Physics D: Applied Physics*, vol. 55, no. 47, pp. 1–10, 2022.

[6] M. Razeghizadeh and M. Pourfath, "First principles study on structural, electronic and optical properties of $HfS_2(1-x)Se_2x$ and $ZrS_2(1-x)Se_2x$ ternary alloys," *RSC Advances*, vol. 12, no. 22, pp. 14061–14068, 2022.

[7] S. Neal, S. Li, T. Birol, and J. Musfeldt, "Chemical bonding and Born charge in 1T-HfS_2," *npj 2D Materials and Applications*, vol. 5, no. 1, pp. 45, 2021.

[8] D. Hoat, R. P. Perez, T. Vu, J. F. RivasSilva, and G. Cocoletzi, "Theoretical analysis of the HfS_2 monolayer electronic structure and optical properties under vertical strain effects," *Optik*, vol. 225, pp. 165718, 2021.

[9] S. Najmaei, C. Ekuma, A. Wilson, A. Leff, and M. Dubey, "Dynamically reconfigurable electronic and phononic properties in intercalated HfS_2," *Materials Today*, vol. 39, pp. 1–5, 2020.

[10] Ali, J. M. Zhang, I. Muhammad, X. M. Wei, I. Ahmad, and M. U. Rehman, "Changing the electronic and magnetic properties of monolayer HfS_2 by doping and vacancy defects: Insight from first-principles calculations," *physica status solidi (b)*, vol. 257, no. 6, pp. 25-35.2020.

[11] Habenicht, J. Simon, M. Richter, R. Schuster, M. Knupfer, and B. Büchner, "Potassium-intercalated bulk HfS_2 and $HfSe_2$: Phase stability, structure, and electronic structure," *Physical Review Materials*, vol. 4, no. 6, pp. 1-8.2020.

[12] K. Obodo, G. Gebreyesus, N. Moro, J. Obodo, E. Ogochukwu, D. Rai, and B. Bouhafs, "Controlling the

electronic and optical properties of HfS_2 monolayers via lanthanide substitutional doping: A DFT+U study," *RSC Advances*, vol. 10, no. 27, pp. 15670–15676, 2020.

[13] N. Taherimakhsousi, B. MacLeod, F. Parlane, T. Morrissey, E. Booker, K. Dettelbach, and C. Berlinguette, "Quantifying defects in thin films using machine vision," *npj Computational Materials*, vol. 6, no. 1, pp. 1–10, 2020.

[14] D. Singh, N. Singh, S. Gupta, and Y. Sonvane, "Effect on electronic and optical properties of Frenkel and Schottky defects in HfS_2 monolayer," *AIP Conference Proceedings*, vol. 1942, no. 1, pp. 1–8, 2018.

[15] H. Lu, Y. Guo, and J. Robertson, "Band edge states, intrinsic defects, and dopants in monolayer HfS_2 and SnS_2," *Applied Physics Letters*, vol. 112, no. 6, pp. 062105, 2018.

[16] D. Wang, X. Zhang, and Z. Wang, "Recent advances in properties, synthesis and applications of two-dimensional HfS_2," *Journal of Nanoscience and Nanotechnology*, vol. 18, no. 11, pp. 7319–7334, 2018.

[17] Yan, L. Gan, X. Zhou, J. Guo, W. Huang, J. Huang, B. Jin, J. Xiong, T. Zhai, and Y. Li, "Space-confined chemical vapor deposition synthesis of ultrathin HfS_2 flakes for optoelectronic application," *Advanced Functional Materials*, vol. 27, no. 39, p. 1702918, 2017.

[18] K. Iordanidou, M. Houssa, G. Pourtois, V. V. Afanas'ev, and A. Stesmans, "Impact of point defects and oxidation on the electronic properties of HfS_2 monolayers," *ECS Journal of Solid State Science and Technology*, vol. 5, no. 11, pp. Q3054–Q3059, 2016.